UNIVERSITYOF
BIRMINGHAM

Application of Positron Emission Particle Tracking (PEPT) for the evaluation of powder behaviour in an incline linear blender for Continuous Direct Compression (CDC)

Jones-Salkey, O; Nicusan, A L; Windows-Yule, C R K; Ingram, A; Werner, D; Clifford, S; Reynolds, G K

Link to publication on Research at Birmingham portal

Application of Positron Emission Particle Tracking (PEPT) for the evaluation of powder behaviour in an incline linear blender for Continuous Direct Compression (CDC)

O. Jones-Salkey [a,c,*], A.L. Nicusan [a,b], C.R.K. Windows-Yule [a,b], A. Ingram [a,b], D. Werner [a,b], S. Clifford [c], G.K. Reynolds [c]

[a] *School of Chemical Engineering, University of Birmingham, Edgbaston, Birmingham, UK*
[b] *School of Physics and Astronomy, University of Birmingham, Edgbaston, Birmingham, UK*
[c] *Oral Product Development, Pharmaceutical Technology & Development, Operations, AstraZeneca, Macclesfield, UK*

ARTICLE INFO

ABSTRACT

Positron Emission Particle Tracking (PEPT) is a non-invasive measurement technique which offers the ability to track the motion of individual particles with high temporal and spatial resolution, and thus build up an understanding of the bulk behaviour of a system from its microscopic (particle level) dynamics. Using this measurement technique, we have developed a series of novel metrics to better understand the behaviours of powders during the steady-state operation of a continuous blender system. Results are presented concerning the response of particle motion to processing parameters (mixing blade configuration and RPM), quantifying the motion in terms of predicted mixing performance. It was found that both increasing rpm and increasing hold-up mass (by selecting fewer transport blades and more mixing blades) provided improved mixing conditions. Interestingly, under specific conditions, there is evidence of convection-like mixing occurring at the interface of the transport and mixing region. This suggests the existence of a potential 'folding region' whereby powder is transported up the barrel (and away from the powder bulk bed) before being reconstituted back into the bulk mass. The results also provide valuable experimental data for the development, calibration and validation of future Discrete Element Method (DEM) simulations.

1. Introduction

In the pharmaceutical industry, the shift from batch to continuous manufacture (CM) carries the potential to significantly reduce both manufacturing cost and product variation (Burcham et al., 2018; Vanhoorne and Vervaet, 2020; Lee et al., 2015; Roth et al., 2017), thus ultimately reducing the cost to the end user, the patient. This mutually beneficial outcome is being pursued by the entire pharmaceutical industry and the authorities are active in parenting the development of these methods (e.g., ICH guidelines (International Council for Harmonisation of Technical Requirements for Pharmaceuticals for Human Use (ICH), 2023, 2012; Wahlich, 2021)), requiring that the introduction of new technologies is sufficiently understood to ensure no risk is passed on to the recipient of these therapeutic products (Bekaert et al., 2022; Lee et al., 2015; Wahlich, 2021).

Therefore, it is paramount that understanding is demonstrated in the form of consistent manufacture (i.e. process design and control strategy) and rigorous models to transition from batch to continuous direct compression (Vanhoorne and Vervaet, 2020; Pernenkil and

Cooney, 2006; Lee et al., 2015). Furthermore, when considering both the complexity of the task and limited of experience manufacturing CM therapeutic products, it highlights that the journey to developing this knowledge is both challenging and costly (Teżyk et al., 2015). Reviews by Wahlich 2021 (Wahlich, 2021) and Teżyk et al. 2015 (Teżyk et al., 2015) both surmise these challenges in greater depth. Wahlich stated that – at the time the review was submitted (June 2021) – only seven CM products were on the market, and of those seven products, they were owned by four companies. As is evident from the above, from both a scientific, regulatory, and commercial standpoint, improved understanding of continuous process equipment is vital to ensuring that the rollout of continuous manufacture can continue in a manner which is both rapid *and* low-risk. The provision of new imaging capabilities stands to play a crucial role in facilitating this understanding.

The continuous direct compression (CDC) process for solid dosage forms (tablets), offers the simplest route to CM by using a minimal number of unit operations to continuously produce tablets. However, our

understanding of how powders respond to mixing process conditions is limited. Excellent examples of work have been conducted by several researchers providing an initial understanding of how bulk powders respond to mixing processes across units with different designs and orientations (Portillo et al., 2010; Vanarase et al., 2013; Van Snick et al., 2017; Palmer et al., 2020; Tomita et al., 2020).

The seminal use of PEPT on small-scale continuous blenders was performed by Portillo et al. (2010), and the findings are discussed later. Vanarase et al. (2013) studied the effect operating conditions had on a horizontal continuous blender through the use of RTD measurements. Van Snick et al. (2017) comprehensively investigated several factors which contribute to end-to-end CDC performance. Where blending is concerned (using a 15° incline blender), Van Snick et, al. demonstrated the influence of blade configuration on mass hold-up and its resultant effect on processing accuracy and consistency — in the form of content uniformity. Palmer et al. (2020) then furthered this by mapping the processing response of three paracetamol formulations and produced a strain micromixing model — which demonstrated an exponential decay between content uniformity (attained from tablet assays) and strain (effectively defined as the number of blade passes). While Tomita et al. (2020) demonstrated the independent control of micro and macro mixing by using a different blender system the CTS-MG100 (Powrex Corporation, Hyogo, Japan), which utilised both a paddle impeller and a circumscribing scraper.

Despite providing considerable insight into mixing processes within CDC, the aforementioned studies nonetheless provide little direct insight into the internal dynamics of the mixing process, due in large part to the optically-opaque nature of the systems studied. Positron Emission Particle Tracking (PEPT) is a technique that uses highly-penetrating gamma radiation to image particulate systems' full, three-dimensional dynamics, including metal-walled industrial process equipment. PEPT is able to track the motion of individual particles through a given system of interest and use these individual traces to build up the understanding of the bulk behaviour of the system, taking a 'micro-up' approach, rather than the typical 'macro-down' approach. Moreover, the spatial–temporal data can be used to calculate a multitude of metrics which are not possible from commonly applied PAT methods, such as NIR, and therefore, PEPT serves as a great tool for investigatory work. Full details of the PEPT technique may be found in Windows-Yule et al. (2020, 2022b).

PEPT has already been used, in the previous work of Portillo et al. (2010), to investigate the effect of RPM and blender inclination on 3 powder species using a small-scale linear blender not dissimilar to that studied here. In their study, it was determined that an inclined blender produced longer residence times and greater mixing potential; the powders travelled similar path lengths but the more cohesive the powder the longer residence time; increasing RPM decreased residence time (lending to poorer macro mixing conditions) but increased radial dispersion — thus increasing the potential mixing quality (Portillo et al., 2010).

An alternative method through which insight may be gained into the internal dynamics of mixing processes is the discrete element method (DEM). DEM, like PEPT, offers a method of understanding the behaviour of not only the bulk but the individual particles within a particulate system. Past studies of such systems have investigated the effect of blade revolution rate (RPM) on axial and radial dispersion (Gao et al., 2011b, 2012) as well as the influence on blade angle on powder transport and mixing (Boonkanokwong et al., 2016; Siraj, 2014; Gao et al., 2011a, 2012; Ebrahimi et al., 2018). DEM offers two pragmatic advantages over PEPT, namely a comparatively low financial cost (due to PEPT's requirement for high energy and materials costs in the production of tracers (Windows-Yule et al., 2022b)) and more ready availability (there exist at present only a handful of active PEPT facilities in the world). However, DEM simulations (depending on the number of particles simulated) will typically take significantly longer than PEPT experiments and, unlike PEPT, DEM simulations may

provide misleading results without rigorous calibration and validation. The necessary calibration and validation thereof is typically complex, time-intensive and lacking a standardised 'best practice', meaning that in many cases such simulations can only be trusted to provide at best qualitative information (Windows-Yule et al., 2016; Windows-Yule and Neveu, 2022). Nonetheless, through careful comparison with detailed experimental data such as that extracted via PEPT or other three-dimensional imaging techniques, near-quantitative accuracy may be achieved (Che et al., 2023).

In this research, we present the first application of Positron Emission Particle Tracking (PEPT) on a commercially-representative, manufacturing-scale continuous blender, following the precedent set by Portillo et al. (2010). Our approach utilises industry-relevant geometries, blade configurations, and RPM ranges. Drawing from the discussions of Gao et al. (2011a) and Van Snick et al. (2017), our goal is to critically analyse how these variables influence the mixing conditions within pharmaceutical blending systems. Our focus, however, is directed towards the micro-behaviour of the powder at the crucial interface between the transport and mixing blade sections of the blender, a region thought to significantly affect the mixing process. In this study, we specifically investigate local factors and their impacts on the *mixing conditions* within the immediate environment, rather than assessing the overall, global, mixing performance. The results obtained from this research will provide meaningful context for our findings and contribute to a broader discussion on *mixing conditions* and regime-like behaviour in similar continuous mixer systems. Moreover, the collected data will serve as an invaluable resource for the rigorous calibration and validation of future Discrete Element Method (DEM) studies.

2. Equipment, materials and methods

2.1. Equipment

2.1.1. Continuous blender: GEA, CDB-1 prototype

Experiments were performed using a prototype of the GEA CDB-1 continuous blender (GEA; Frankfurt, Germany). The blender's mixing volume is angled at a 15-degree incline from the inlet to the outlet so as to increase the total hold-up mass as compared to an equivalent, horizontal system. The internal diameter of the blender is 118 mm and the mixing volume of the blender is 9.3L. The blender has the same mixing dimensions as its commercial counterpart but is more modular in its assembly. The blender's axial shaft has 28 collars, each of which accepts two blades which can either be at 45 degrees to the axis (push blades) or 90 degrees to the axis ((radial) mixing blades). The mixing configuration is set up such that each collar is offset from the preceding collar by 60 degrees thus the progress of the mixing blade(s) moves as a helix along the shaft. The helix rotation provides positive movement in the direction of flow. The two configurations used for this experiment are '8H' (8 mixing blades) and 16H (16 mixing blades), meaning that the mixing section covers roughly 25 and 50 per cent of the shaft, respectively. Schematic representations of the two blade configurations explored can be seen in Fig. 3. The system is controlled using a variable frequency drive allowing the user to manually control the RPM. The rotation rate was measured using a CT6/LSR laser tachometer (Compact Instruments, Bolton, UK) with a contrasting marker on the drive shaft. The rotation rate of the shaft is measured and the drive frequency is adjusted accordingly.

2.1.2. Twin screw feeder: Coperion, KTron-20

For all experiments, particles were fed into the blender using a KTron-20 Feeder (Coperion; Stuttgart, Germany) with concave screws. The feeder was calibrated prior to use, ensuring a consistent volumetric feed over a range of hopper fill levels and screw RPMs. All experiments used a volumetric feed rate equivalent to 15 kg hr^{-1}. This feed rate was the highest feed rate which provided a consistent mass flow rate. Due to the age of the feeder, and therefore the settings available,

only volumetric feeding was possible. The calibration gave confidence in operating volumetrically over the full range of hopper fill levels. This is primarily attributed to the free-flowing nature of the powder. Consequently, the feed rate remained accurate and stable across all experiments.

2.1.3. PEPT detector: ADAC, PET scanner

Data were acquired from the experimental system using an ADAC Forté dual-headed gamma camera. The camera offers a peak acquisition rate of approximately 100 kHz Parker et al. (2002) and, with modern algorithms (Windows-Yule et al., 2022a), can compute the three-dimensional position of a tracer particle with sub-millimetre accuracy more than 100 times per second. Full details of the Forté can be found in Parker et al. (2002), Herald et al. (2021).

2.2. Materials

2.2.1. Bulk & tracer material: 1 mm MCC

A coarse microcrystalline cellulose (MCC), Vivapur 1000 (JRS Pharma; Rosenberg, Germany), was selected as both the bulk material and the tracer for this experiment. The primary advantage of this material is its narrow particle size distribution and average particle diameter of 1.2 mm; this large particle size provides a greater surface area which is desirable for improved radioactive labelling tracer performance. The large size of the particles also reduces the total number of particles within the system, thus making our results more viable as a calibration/validation data set for future DEM simulations. Furthermore, the selected powder is a pharmaceutical-grade material and is free-flowing (Zheng et al., 2022); which would be representative of a low-dose API formulation, as many excipient formulations prioritise flowability for improved manufacturability (Megarry et al., 2019; Jones-salkey et al., 2023).

Lastly, the tracer was created via the surface adsorption of the positron-emitting radioisotope Fluorine-18 (^{18}F). Details of this procedure, known as 'indirect activation' can be found in Windows-Yule et al. (2022a).

2.3. Experimental set-up

Since the blender is commercial scale, with a length of 0.85 m, the blender does not fit fully within the maximum 0.55 m field of view (FoV) of the detector. With the 15-degree inclination of the blender, the total length that fits within the FoV is 0.57 m or 67% of the blender's length. For the purposes of the present study, imaging of the interface between the mixing blade zone and the former transport section is of primary interest. This volume is expected to contain more than 80% of the residence mass; supported by the comprehensive DEM work of Zheng et al. (2022), which showcases analysis of a simulation calibrated for the same blending volume and powder — Vivapur 1000.

Thus, the inlet of the blender was positioned at the start of the FoV with the interface of the smaller mixing blade zone (8H) being captured by the end of the FoV. The finalised FoV was 0.5 m (in the length axis), and the interface was prioritised within the FoV (which spanned from 0.22 m to 0.42 m). The region of interest for calculation is shown with greater clarity with the following: Fig. 2.

The blender sits, fastened, within the middle section of a two-tiered extruded aluminium frame. The upper section of the frame accommodates the feeder, which is bolted in place (see Fig. 1). The aluminium frame, and therefore the blender, is kept stationary within the detector heads of the ADAC for all experiments. The ADAC detector head separation is then narrowed in the width axis ensuring the highest possible geometric efficiency (i.e. the largest fraction of gamma-rays detected) and thus in turn the maximal data rate and location accuracy (Windows-Yule et al., 2022a; Herald et al., 2021).

Fig. 1. Picture of the Experimental Set-up; supporting frame holding the blender and feeder in the ADAC detector's FoV.
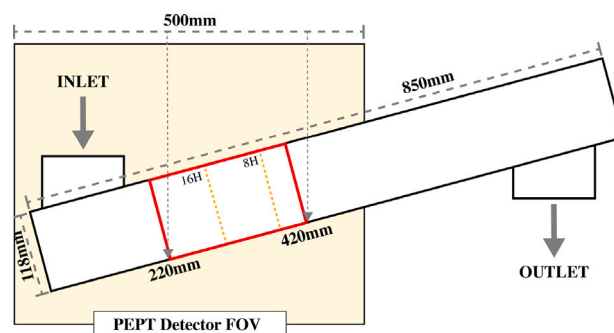

Fig. 2. Schematic of the Experimental Set-up; showing the blender, and the dimensions, within the ADAC detector's FoV. The Region of Interest (RoI) is indicated by the red box.

2.4. Experimental design

In this study, we explore two variables: the blade revolution rate (RPM), and the number of mixing blades (#MB). Increasing the number of mixing blades has been previously shown to increase the overall fill level (residence mass) of such a mixer system, while increasing RPM has been shown to reduce the fill level (Van Snick et al., 2017; Palmer et al., 2020). By varying both of these parameters, we are able to explore a range of system fill levels, and thus gain understanding of the behaviour of powder under strongly varying conditions.

It was found that the combination of low speed and reduced transport resulted in high material hold up, and consequently the torque required exceeded that deliverable by the motor. For this reason, the lowest speed used for 16H is 225rpm. This, coupled with the limited amount of time available to perform the PEPT experiments, means the analysis includes only the following data sets: 150 RPM at 8H, 375 RPM at 8H, 225 RPM at 16H, 300 RPM at 16H, and 375 RPM at 16H.

2.5. Experimental method

The blade configuration is set to the desired configuration and installed into the blender. The blender is subsequently turned on and set to the desired RPM whilst filling. The MCC is then added to the feeder and set to run at 15 kg/hr. While the blender is filling, using both the variable frequency drive and the tachometer, the frequency is adjusted until both remain constant. When the torque (and therefore
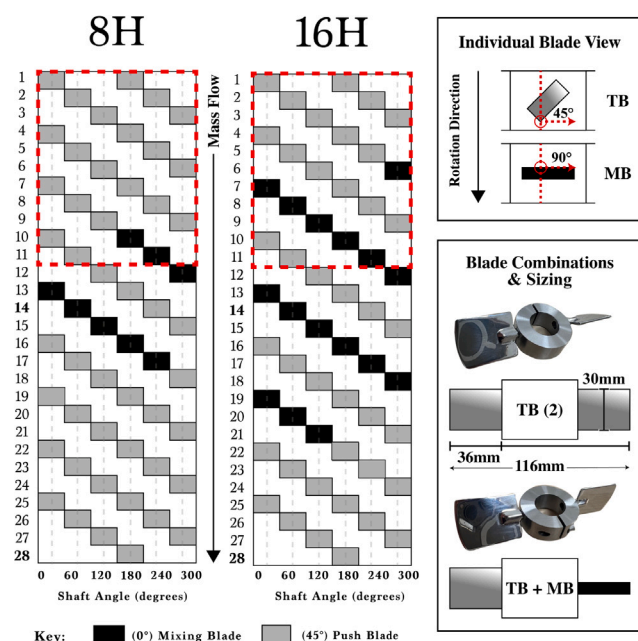
Fig. 3. Blade dimensions and angle arrangement for the 8H and 16H configurations. The red dashed-line box indicates the FoV of the detector.

rpm) remains constant, there is an equal amount of mass entering and exiting the system, effectively stating the system is at steady state due to the constant load on the blades. To ensure the system was at steady state; the system was monitored for a further 5-minute period, in which the rpm was regularly monitored for consistency.

Once at steady state, the tracer is then directly inserted into the neck of the feeder, bypassing the hopper, and enters the blender. A bucket collects the powder output of the blender and is returned to the hopper of the feeder when the tracer is detected in the bucket. This is repeated to gather a sensible number of passes through the system. The data is then processed using the method in the following section (Section 2.6.1). Finally, the residence mass (hold-up mass) of each experiment was estimated by weighing the powder remaining in the system at the end of the trial.

2.6. Analysis

2.6.1. Extracting and cleaning individual trajectories

In order to acquire data with the maximum spatial resolution, tracers are passed through the system one at a time. Though PEPT is capable of tracking multiple tracers simultaneously (Yang et al., 2007; Nicuşan and Windows-Yule, 2020), doing so reduces the accuracy with which each individual particle may be located, meaning that single-particle tracking provides optimal data (Windows-Yule et al., 2022a). In order to build up adequate statistics, therefore, for each set of system parameters, a single tracer is repeatedly passed through the system. By exploiting the principle of ergodicity, data acquired from a series of individual transits of the tracer particle through the mixer (for brevity referred to throughout this paper as 'trajectories') may be combined and suitably averaged so as to provide data representative of the system as a whole (Wildman et al., 2000).

As the detector does not encompass the complete system, there is a possibility that during the tracer's full pass through the system, the tracer may leave and re-enter the field of view, thus potentially being erroneously considered as multiple individual trajectories, creating small, fragmented data sets towards the extremes of the Field of View (FOV) which, if incorporated into statistical analyses, may adversely bias results. Accordingly, filtering measures were put in place

to uphold the integrity of those tracers which have truly re-entered due to back-mixing and expelling the erroneous traces. As such, methods were developed to algorithmically remove such fragmented data sets in pre-processing by Firstly, any data sets possessing an overall location error above a given threshold – as expected to be produced by tracers outside the field of view – were eliminated. Secondly, any trajectories containing < 120 contiguous data points – implying only a partial transit – were eliminated. Thirdly, only trajectories containing data points spanning at least the central 200 mm (50%) of the system's field of view were included in our analyses, capturing the interface between transport and mixing blade zone.

Once all erroneous data sets had been eliminated, the remaining trajectories in each experiment were then subjected to a series of 'post-processing' analyses. Due to the sparsity of the data acquired – an inevitable consequence of the complexity of the system and the limited experimental time available – in addition to conventional PEPT outputs such as occupancy and velocity fields, a number of novel metrics were developed specifically for this project. These metrics are described in the following sections.

2.6.2. Novel analyses

Traversal classification. During preliminary analysis, it was observed that the observed particle trajectories could be reasonably classified into three primary 'blender traversal modes':

1. Centrifuging: particles remain at the outer edge of the blender, resulting in bulk rotation about the unit's central axis with minimal transport along the radial direction. This is not to be confused with centrifuging observed in rotating drums where the powder bed attaches to the wall as a solid body with no relative movement between particles. In this case, the particles are held at the wall by action of the rotating blade.
2. Axial traversal: particles pass through the blender with minimal motion in either the radial or azimuthal directions, resulting in relatively short, straight trajectories.
3. Random motion: particles are actively entrained between the blades, resulting in stochastic axial and radial motion (i.e. a random trajectory).

This novel analysis has been included in the present work since we believe that the different behaviours will represent different mixing mechanisms and different mixing efficiencies. Further work is required to explore this, but it is certainly arguable that the random motion mode would lead to effective mixing while that of the axial traversal mode would be quite poor, hence undesirable in pharmaceutical blending applications. The centrifugal mode is less clear cut; it requires knowledge of the motion of the particles relative to the blade and hence the relative extents of the blade pushing the bed of particles (convective motion, poor mixing) versus shearing through (dispersive motion, good mixing). Identifying the prevalence of these behaviours for different processing conditions can thus play a role in the optimisation of said conditions.

To ensure rigour, an algorithmic approach has been taken to the classification of trajectories. In order to classify a given trajectory, the following considerations are applied:

1. The PEPT tracer locations are rotated by $-15°$ and centred such that the main blender body lies horizontally, with the X-axis passing through the centre of the shaft.
2. Each trajectory's points are converted to cylindrical coordinates, with the longitudinal (shaft) axis corresponding to the Cartesian X-axis, such that the YZ coordinates are transformed into a radial distance r and an azimuthal angle θ.
3. In perfect centrifugal motion, the distribution of azimuthal angles will be uniform between $[-\pi, \pi]$ and hence their standard deviation will be $\sigma_\theta = \pi/\sqrt{3}$, while the radial position r will
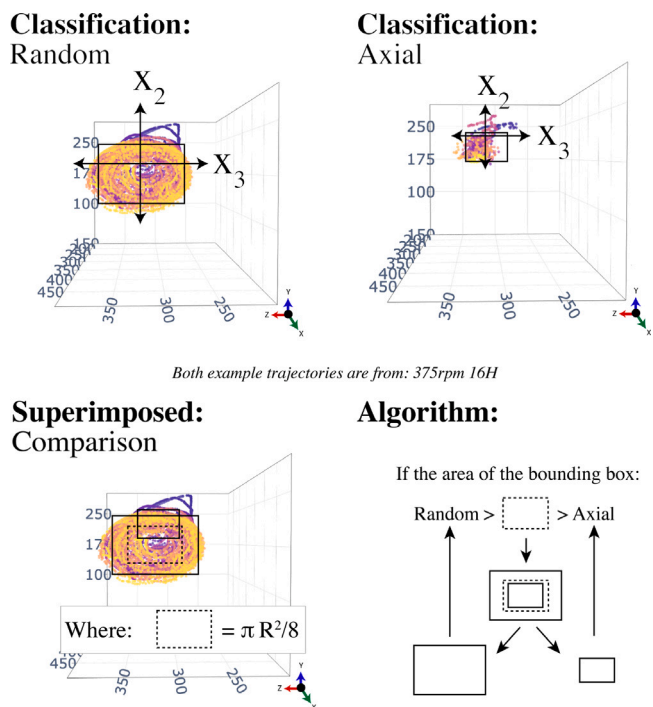
Classification:
Random

Classification:
Axial

Both example trajectories are from: 375rpm 16H

Superimposed:
Comparison

Algorithm:

If the area of the bounding box:

Fig. 4. Graphical supplementation of the axial classification calculation. The units of the 3D scatter plots are in millimetres. Overlayed examples are not to scale.

be equal to the blender radius. Empirically-defined thresholds are used, such that if $\sigma_\theta < 0.75\pi/\sqrt{3}$ and the 25th percentile of a tracer pass' radial distances is greater than half the blender radius $P_{25\%}(r) > R/2$, the trajectory is classified as centrifuging.

4. Axial motion corresponds to minimal blade entrainment, such that the tracer radially explores a small area of the pipe; we extract the plane orthogonal to the main axis of flow by converting each trajectory's points' coordinates into their principal components' space (PCA, using the eigenvectors of their covariance matrix) and extracting the coordinates of the two least important axes X_2 and X_3 (note that the most important axis X_1 corresponds to the main flow direction); the area spanned by the 5th to 95th percentiles $A = (P_{95\%}(X_2) - P_{5\%}(X_2))(P_{95\%}(X_3) - P_{5\%}(X_3))$ robustly approximates the radial side of an oriented bounding box containing the trajectory's points, without outliers — and hence the radially-explored area. As the principal components X_2 and X_3 still have physical units, their dimensions can be compared with that of the blender. If the computed area A is smaller than a blender octant $A < \pi R^2/8$, the trajectory is classified as an axial traversal. This (axial) classification is supplemented graphically by Fig. 4.

5. Finally, all remaining trajectories are considered to undergo random mixing.

In other fields of study, for example in rotating drum systems, the classification of particle motion provides a valuable tool for the inference of mixing quality and other important parameters (Morrison et al., 2016). It is hoped that these classifications may prove similarly valuable in the pharmaceutical mixing field.

Lagrangian micromixing. As more industrial systems are imaged using Lagrangian techniques offering rich three-dimensional information of their internal dynamics, new mixing measures must be developed beyond the classical approaches in chemical engineering. A novel method for quantifying the radial movement of flow specifically targeted to
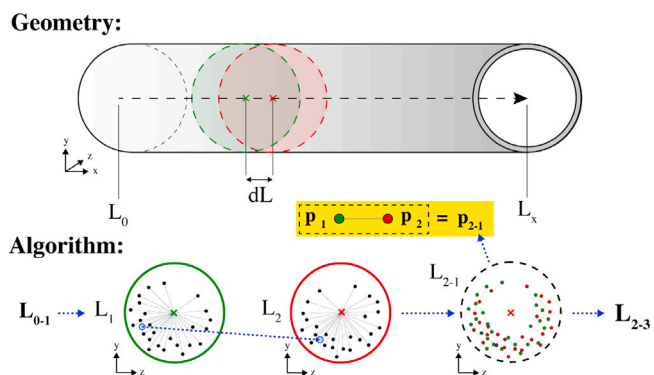
Geometry:

Algorithm:

Fig. 5. Graphical Representation of the Lagrangian micromixing metric discussed in Section 2.6.2.

moving frames of reference (i.e. Lagrangian data) has been developed, providing richer information regarding the 'microscopic' mixing (Werner et al., 2023) of tracer particles. The algorithmic steps are as follows (supplemented by Fig. 5):

1. Take a cross-sectional slice through the blender at length L_1 (axial position) along it and record each tracer's location as it passes through the slice.
2. On this slice, compute the radial distances from each trajectory to the pipe centre ($r_1^{L_1}, r_2^{L_1}, \ldots, r_N^{L_1}$) for N tracer passes.
3. Take a second cross-sectional slice at a later length L_2 along the blender and similarly compute the new radial distances ($r_1^{L_2}, r_2^{L_2}, \ldots, r_N^{L_2}$).
4. Compute the *radial deviations* due to micromixing ($r_1^{L_2} - r_1^{L_1}, r_2^{L_2} - r_2^{L_1}, \ldots, r_N^{L_2} - r_N^{L_1}$).
5. Quantify the distribution of radial deviations through its mean, standard deviation, skewness and kurtosis.
6. Move the second slice, L_2, to a new position further along the blender and repeat steps 3–5, keeping track of the radial deviations' statistics as tracers pass through the mixing region.

This method is robust to both axial and centrifuging types of trajectories, as: if tracers follow laminar-like straight trajectories, the mean radial deviation will be zero; if tracers follow the (centrifugal) bulk rotation, it will again be zero. This way, only *true micromixing* is captured by the Lagrangian Micromixing metric. Specifically, a larger mean value corresponds to stronger micromixing, with the standard deviation representing the mixing uniformity. A larger skewness (i.e. a longer right tail on the distribution) indicates that only a few tracers are mixed well; finally, a negative kurtosis suggests the presence of a small number of mixing outliers.

Auto-correlation. Auto-correlation within PEPT has been generalised from the molecular dynamics' velocity auto-correlation function (VACF) (Leimkuhler and Matthews, 2015), defined as the ensemble average – across N trajectory passes – of the dot product of a vector quantity (e.g. velocity $V = (v_x, v_y, v_z)^T$) measured at an initial time t_0 and the same vector quantity measured at a later time t_i:

$$\text{VACF}(t_i) = \frac{\sum_N (V(t_0) \cdot V(t_i))}{N} \tag{1}$$

The time can be substituted with any 'signal' S that has a lag added to it, e.g. position along the blender, in which case it represents the correlation C of a vector quantity $\vec{Q}$ as tracers traverse the mixing region:

$$C(S_i) = \frac{\sum_N (\vec{Q}(S_0) \cdot \vec{Q}(S_i))}{N} \tag{2}$$

Table 1
Tracer classification based on the definitions provided in Section 2.6.2, followed with the number of trajectories collected.

Blender parameters	8H		16H		
	150	375	225	300	375
Froude No.	1.5	9.3	3.4	5.9	9.3
Axial	48%	4%	18%	25%	20%
Centrifugal	0%	73%	0%	2%	10%
Random	52%	23%	82%	73%	70%
n-trajectories	23	271	66	51	93

High auto-correlation indicates that tracers strongly follow a trend, while zero auto-correlation represents unpredictable, or randomly-distributed values; for example, as tracers are being mixed along the blender, their coordinates (x, y, z) are expected to become less correlated and hence C to decay to zero.

While *velocity* auto-correlations have been previously applied in PEPT studies of *batch* systems (Wildman et al., 2002; Windows-Yule et al., 2014), the present work develops a new formulation for continuous systems, and generalises the algorithm to allow the auto-correlation of arbitrary parameters to be computed.

Algorithm availability. All algorithms described in this section are freely available through the authors' open-source `pept` library (see https://github.com/uob-positron-imaging-centre/pept).

2.6.3. Classical analyses

In addition to the novel analyses defined above, data were also obtained in the form of spatial residence time distribution (otherwise described as temporal occupancy) and velocity profiles, providing further insight into transport and mixing within the system, and the dependence thereof on process conditions.

The methodology for attaining these standard measurements can be found in Windows-Yule et al. (2020, 2022b).

3. Results & discussion

In order to improve CDC processes, it is vital that we are able to better understand – and thus predict and, ultimately, control – processes underlying both the micro- and macro-mixing of powders. While previous studies have elucidated correlations between the 'input' process parameters and the bulk response of the system, the use of PEPT in the current study offers insight into the system's microscopic response. This not only offers a direct insight into the micro-mixing behaviours of the system studied but also carries the potential to provide a greater mechanistic understanding of the previously-observed macroscopic behaviours.

In the following section, we use the analysis methods described in Section 2.6.2 to provide both Lagrangian and Eulerian data providing insight – both direct and indirect – into the mixing dynamics of our incline blender system, and their variation with key system parameters.

3.1. Traversal classification

Table 1 (and Fig. 6 graphically) show, for each combination of blade rotation rate and mixing blade number explored, the percentage of recorded trajectories classified as 'centrifuging', 'axial traversal' or 'random motion' based on the criteria described in Section 2.6.2. As noted previously, random motion is expected to be desirable in terms of mixing, while both axial traversal and centrifuging trajectories, which limit transport in one or more directions, are expected to be detrimental. Classified example trajectories can be seen in Fig. 7

As one may intuitively expect, there is a clear positive correlation between the percentage of centrifuging trajectories and the blade RPM, and thus the Froude number, which for our purposes we define as:
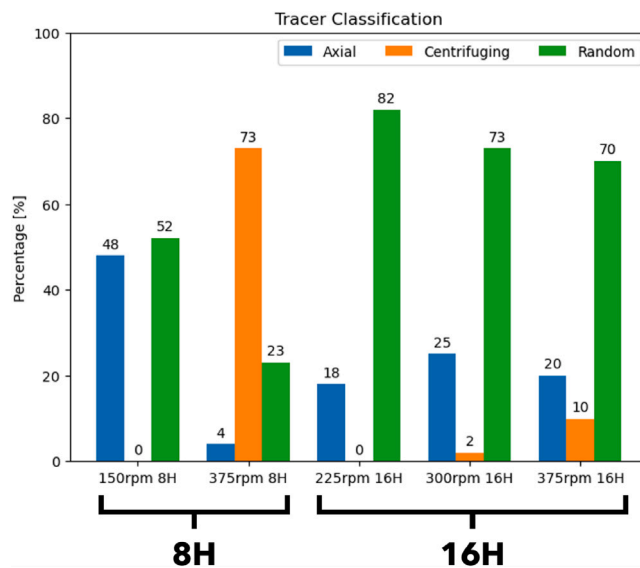
$$\text{Fr} = \frac{\omega^2 R}{g} \qquad (3)$$

Fig. 6. Graphical Representation of Table 1 discussed in Section 3.1.

where ω is the blade rotation rate in radians per second, and R is a relevant length-scale, here the radial length of a blade — i.e. the distance from the centre axis of the system to the tip of a given blade.

Interestingly, at equivalent blade rotation rates, the percentage of centrifugal trajectories is significantly reduced for the 16H case as compared to the 8H case, strongly suggesting that the presence of (more) mixing blades acts to suppress this undesirable transport modality.

The relationship between the system parameters and the recorded number of axial traversal-type trajectories is less clear-cut. For an 8H configuration, the data emphatically show that a low rotation rate produces a large number of such trajectories; and that this number is significantly reduced at higher rotation rates. However, this positive reduction is more than outweighed by the substantial increase in centrifugal trajectories. For the 16H case, the number of axial trajectories remains constant, to within experimental error margins, for all RPM tested.

Finally, if we consider the prevalence of (desirable) 'random' trajectories, we see immediately that an increased number of mixing blades is preferable, with the overall fraction of such trajectories higher for all 16H cases than for either 8H case explored. Within the 16H cases, there appears to be a weak negative correlation between blade RPM and the percentage of 'good' trajectories. As such, based on considerations of mixing alone, a lower RPM seems desirable. However, considering the comparatively weak relationship observed, when considering also throughput, a faster rotation rate may in fact be desirable.

3.2. Lagrangian micromixing

As described in Section 2.6.2, the Lagrangian Micromixing metric provides information regarding the overall strength of micromixing, illustrated by the mean 'Deviation' values presented in Fig. 8, as well as the uniformity with which mixing is achieved across different regions of the system, illustrated by the standard deviation thereof. As such, strong and consistent mixing is represented in Fig. 8 by a large mean with a wide distribution. This method would be categorised as a distance-based method within Bhalode and Ierapetritou's review on continuous solid-based mixing indices (Bhalode and Ierapetritou, 2020); which comprehensively showcases a plethora of useful comparable mixing indices across a range of publications.

The data presented in Fig. 8 strongly indicate that the 375 RPM, 16H case provides both the strongest and most uniform micromixing, showing also – as one may intuitively expect – an increase in the
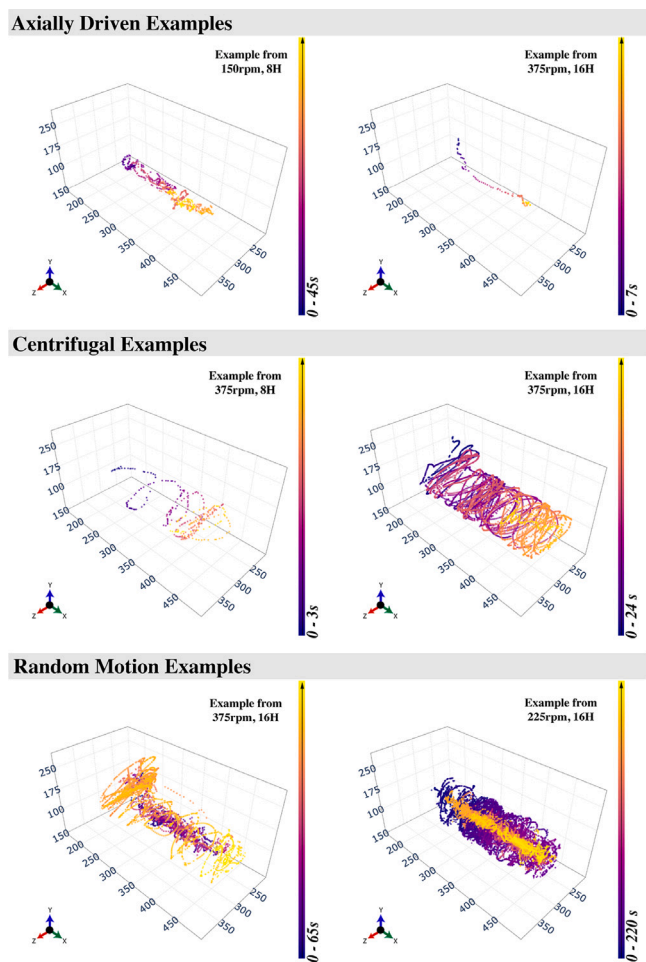
Axially Driven Examples

Centrifugal Examples

Random Motion Examples

Fig. 7. Example tracers plotted in 3D (with units mm), where each trace is labelled by its corresponding classification, RPM and blade configuration. While the colour bar indicates the time in seconds.

Fig. 8. Lagrangian micro mixing along the axis between: Point 1, 220 mm and Point 2, 420 mm. The Mixing Blade Zone (MBZ) starts at 310 mm and 390 mm for the 16H and 8H configurations respectively.

micromixing parameter within and immediately adjacent to the mixing blade zone (MBZ). Curiously, this uptick in micromixing within the MBZ is not clearly observable within the other data sets. From the figure, we see also that the poorest mixing performance is observed for the 150 RPM, 8H case.

The system with the greater number of mixing blades and the highest RPM (i.e. more energy imparted to the system) results in the highest value for the micromixing parameter (an indication of the speed at which particles are expected to diverge from one another), while that with the fewer blades and the lowest RPM yields the lowest value, again makes physical sense on a fundamental level. The existence of a correlation between RPM and the micromixing of particles has been previously demonstrated (for a horizontal system) by the numerical simulations of Sarkar & Wassgren 2009 (Sarkar and Wassgren, 2009), who investigated the variation of a dimensionless radial-plane dispersion index as a function of the Froude number and mixer volume-fill. For lower (< 0.5) fill fractions, a positive correlation was observed between the dispersive index and the blade revolution rate, though at higher fill levels the inverse was observed. As, due to the relatively low feed-rate of our system, a comparatively low average fill height was achieved in our systems, our results are broadly in line with the expectations of this prior work.

Furthermore, by abstracting Sarkar & Wassgren's (Sarkar and Wassgren, 2009) findings for this inclined system (compared to their horizontal system), it would be sensible to map this similar behaviour to the blender — i.e. considering an environment in which the fill level
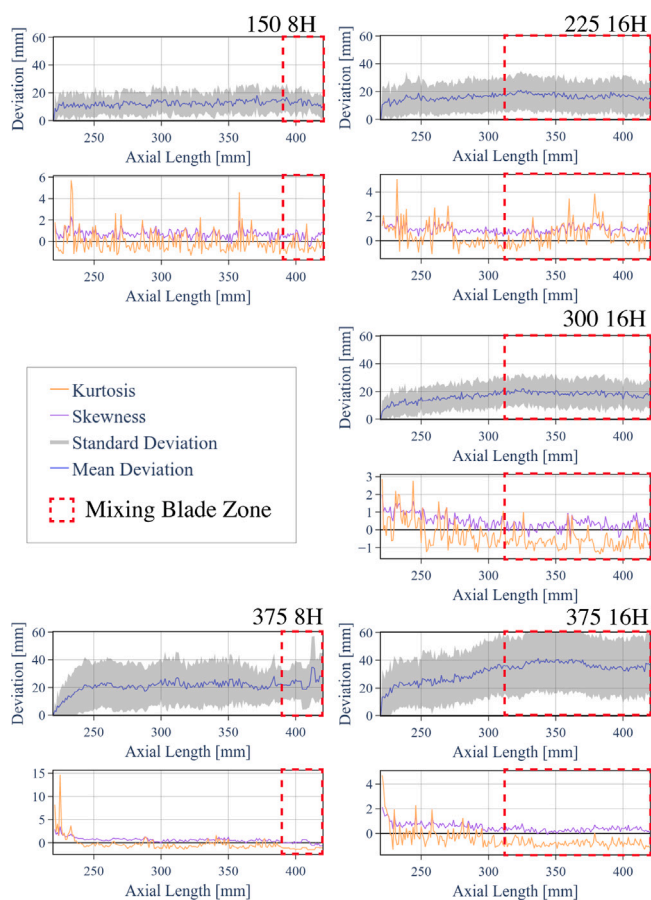
(and therefore, the radial-plane dispersion) would vary down the length of the barrel. By Sarkar & Wassgren's (Sarkar and Wassgren, 2009) measures, the 8H at 375 RPM should show the greatest radial-plane dispersion index and therefore the greatest mixing performance, as it would have the lowest fill with the highest Froude.

Conversely, the results of Van Snick et al. (2017) – who use a blender with the same geometry as this study – show that configurations with fewer mixing blades and thus lower residence mass provide poorer mixing outcomes than configurations which hold greater residence mass. The results from the lagrangian micromixing (Fig. 8) align well with Van Snick et al.'s findings — but also suggest that there is further complexity associated with the interaction between fill level (residence mass) and Froude number RPM. It should be noted the differences in inclination between the two studies ($0°$ and $+15°$, from the horizontal respectively), however, the pure comparison between fill level and RPM on the dispersion performance, contradict one another. Highlighting the fact that the underpinning behaviour is still poorly understood. Employing methodologies like the lagrangian micro mixing help elucidate both the local behaviour and regional behaviour along the length of the barrel — effectively describing radial dispersion as a function of conditions experienced along the axial length.

3.3. Auto-correlation

The autocorrelation functions presented in Fig. 9 illustrate the rate at which the radial positions of particles become decorrelated from their initial values as a function of the distance, x, travelled along the blender axis. A value of $C_r(x) = 0$ thus indicates chaotic,
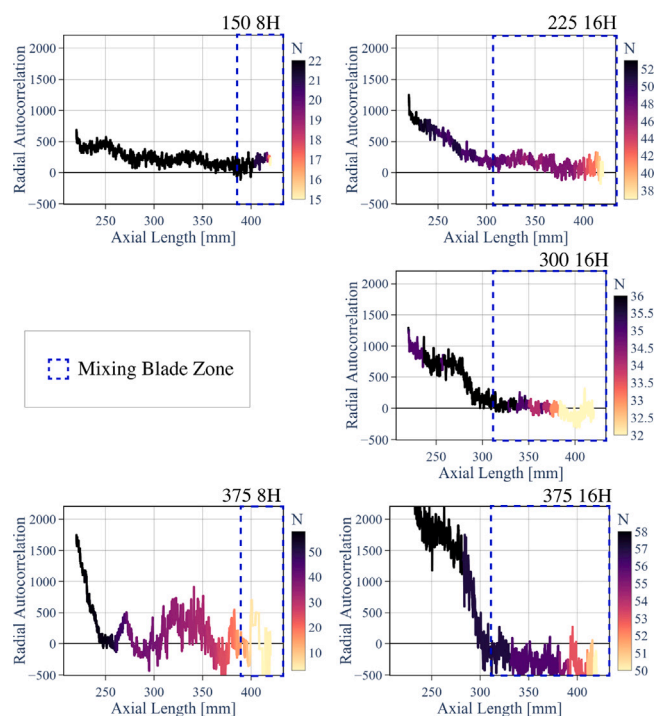
Fig. 9. Auto-Correlation ($C_r(x)$) of the $[y, z]$ radial plane as a function of $[x]$ the axis length. Detailing predictability of the radial position along the barrel. $AC = 0$ shows no predictability between the radial and axial plane, suggesting a high level of radial dispersion. N is the number of traces in the AC calculation, and therefore an indicator of confidence.

history-independent behaviour (Baxter and Olafsen, 2007), making it a valuable proxy measurement for mixing.

For all cases investigated, we see a general decrease in $C_r(x)$ as the distance from the inlet increases, indicating an increase in mixing. For the 16H cases in particular, we note that $C_r(x)$ decreases to approximately zero within the mixing blade zone, indicating the presence of strong, chaotic mixing in this region — as one may inherently expect.

Cross-comparison of the autocorrelation data shown in Fig. 9 with the residence time profiles presented in Fig. 10 shows that this behaviour coincides with a distinct peak in occupancy indicative of a 'pile-up' of material at the interface between the 'push-blade' zone and the mixing blade zone which is not present in the other data sets. The presence of this additional mass hold-up suggests a region of back-mixing or 'folding' as the fast-moving particles from the push-blade region meet the slower-moving MBZ, thus creating in essence an extended 'effective mixing region'.

The 'folding region' is shown by the 16H blade configuration at 300RPM and 375RPM, identified by the combination of key 'signatures' in both the autocorrelation (AC)(Fig. 9) and the spatial residence time (Fig. 10) at axial length 290 mm. Specifically, in the presence of a folding region we expect a sharp drop in the radial correlation combined with a significant increase in hold-up before the mixing blade interface. The simultaneous expression of these describes a behaviour where axial transport is converted into the radially promoted section, resulting in the powder now undergoing an increase in dispersive radial mixing, but also an increase in the probability that the powder will slip back down the barrel, providing also a remixing effect in the axial direction, mimicking the behaviour in a rotating tumbler (Morrison et al., 2016). The tumbling and reconstitution of powder within a rotating-drum mixer, or indeed the convective remixing inside a bubbling fluidised bed, are both known for their ability to promote both micro- and macro-mixing (Werner et al., 2023) and, as such, we may reasonably expect a similar effect here.

In the case of the 225 RPM, 16H system, this 'folding region' is seemingly absent, likely due to a reduced differential in the transport rate between the push-blade and mixing-blade zones at lower RPM. In this instance, $C_r(x)$ does not reach 0 until well within the MBZ. Such a zone is also absent from both 8H cases.

Unlike the 16H cases, which show a generally monotonic decrease in $C_r(x)$ with x, the 8H data sets – in particular the 375 RPM, 8H case – show an autocorrelation function which oscillates on a relatively large length scale, indicating that the particles – or at least a subset thereof – retain some degree of 'memory' of their initial conditions even after they have travelled a significant distance through the system (Campbell, 1997). This observation ties in well with our earlier finding (Section 3.1) that the 150 RPM, 8H and 375 RPM, 8H cases elicit, respectively, a large number of axial traversal and centrifuging trajectory modes.

Finally, it is worth noting that calculating the autocorrelations both for a constant initial position with varying lag (as presented in Fig. 9) and constant lag with varied initial position showed similar results, indicating the robustness of our observations.

3.4. Axial spatial residence time distribution

The spatial residence time profiles presented in Fig. 10 illustrate the relative fraction of time spent by tracers, on average, within different axial regions of the system. We have already described, in Section 3.3, the tendency of the higher-RPM, 16H to produce a hold-up region at the interface of the push-blade and mixing zones, and the absence of such a region in the lower-RPM case.

In the 8H cases studied, no hold-up region is observed for either blade rotation rate, and – unlike the 16H cases – the difference in residence between the push-blade zone and mixing-blade zone is stark, in particular for the 375 RPM case, where the minimal occupancy in the former region indicates an extremely rapid transit therein. This observation once again ties in well with previous observations (Sections 3.1 and 3.3) suggesting a tendency for tracers to take a direct path through the system (either axially or centrifugally) rather than experiencing any significant back-mixing.

We expect these distributions to change significantly, depending on the bulk material's characteristics and processing conditions. Moreover, it would be interesting to investigate whether the spatial residence time distribution remains the same for materials operating with equal strain; where strain is described as the number of blade passes multiplied by the mean residence time. If true, it would show evidence of mixing being influenced by regime-like behaviour within the blender — which may be a parameter to optimise.

4. Conclusion

In this study, we have used positron emission particle tracking (PEPT) to investigate the underpinning particle-level (microscopic) behaviours of a simple pharmaceutical powder in a commercial-scale incline linear blender. Data are obtained for a variety of blade rotation rates and two distinct blade configurations, including either 8 or 16 'mixing blades' (oriented, as their name implies, to encourage mixing) with the remainder of the system occupied by 'push blades' (oriented to encourage transport).

Leveraging the unique capabilities of PEPT to extract Lagrangian information from particulate systems with high temporal and spatial resolution, we have developed a series of novel metrics to probe and quantify the powder's dynamic response to differing process parameters in an incline linear blender.

Firstly, we have developed a set of algorithms through which the trajectories of particles through the system may be classified as either 'random motion' (desirable for mixing) or 'centrifuging' or 'axial' motion (less desirable). Knowledge of the existence of these less-desirable modes, not previously been documented in the literature, may prove
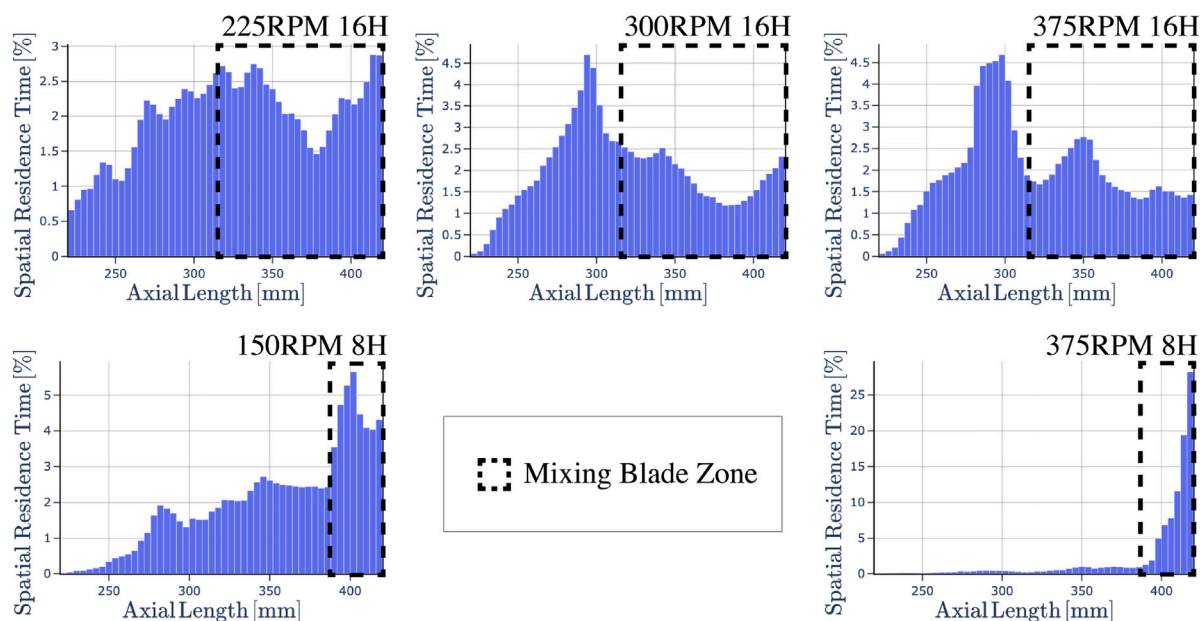
Fig. 10. Spatial Residence Time plots, normalised by the area under the graph, for the various speeds and their given blade configuration. The region of interest for the calculation spans between 220 mm to 420 mm. A black dashed line denotes the Mixing Blade Zone and corresponds to where the mixing zone starts along the axial length (mm), the zones start at 310 mm and 390 mm for the 16H and 8H respectively. To remove any erroneous tracers, a filter was applied to the calculation excluding points which had; traces shorter than 200 mm, min velocity of 0.01 m/s, max velocity of 3 m/s, and points with relative error >95th percentile.

valuable to industrial users of continuous blenders, who will naturally want to avoid the process conditions which give rise to them.

Our results show that the '8H' systems – those possessing a lower number of mixing blades – exhibited a larger number of less-desirable transit modes than the '16H' systems, with a shift from axial to centrifuging motion as the blade rotation rate is increased. For the 16 mixing blade case, we observed a similar increase in the percentage of centrifugal trajectories, though this apparent shift is less statistically significant.

Secondly, we have introduced a 'Lagrangian Micromixing' metric, similar in interpretation to the more conventional 'dispersion' metric used in prior PEPT studies (Martin et al., 2007; Windows-Yule et al., 2020) but capable of handling sparse, discontinuous data in rotating reference frames. The data obtained using this metric suggest that the 16 mixing blade system at the highest test blade rotation rate exhibited the strongest (micro)mixing conditions, with the 8H case at the lowest RPM producing the weakest (micro)mixing conditions.

Finally, we have developed a generalisable PEPT auto-correlation function suitable for continuous systems. As the autocorrelation function employed can be meaningfully interpreted as a measure of order and thus, by definition, an indicator of the presence of chaos, it provides another valuable predictor of mixing. This parameter once again indicates that improved mixing conditions may be achieved with more mixing blades and at a higher RPM. These data, combined with additional data in the form of spatial residence time distributions, show the existence of a high-hold-up 'folding region' at the interface of the push-blade and mixing blade regions, creating in essence an extended mixing zone. This folding region is observed only for the 16-blade configuration at relatively high ($\gtrsim$300 RPM) blade rotation rates.

Overall, our results suggest that – for the range of parameters tested – improved mixing conditions may be achieved for the combination of more mixing blades and higher RPM. The positive influence of high blade rotation rate in particular is a potentially pleasing finding for the field, as it reduces the need for a compromise between mixing quality and throughput. Nonetheless, these data were acquired only using a comparatively simple, non-cohesive powder, and a relatively low feed rate and (thus) fill fraction. Further work should be performed using additional materials and feed rates in order to assess the generality of our results.

It is important to keep in mind that more mixing or improved mixing conditions may not always have a positive effect. In the case of powder lubrication with, for example, magnesium stearate, over-zealous mixing may lead to over-lubricated tablets; which then result in reduced tablet tensile strength (Mosig and Kleinebudde, 2015) and slower disintegration/dissolution rates (Nickerson et al., 2018). Therefore, processing parameters like the 8H (at high speed) may be better suited for a given formulation and specific use case.

In addition to the information gained directly from our results, the detailed, three-dimensional data obtained provide a valuable calibration/validation data set for future DEM models of continuous blender systems (Windows-Yule and Neveu, 2022).

CRediT authorship contribution statement

O. Jones-Salkey: Conceptualization, Data curation, Formal analysis, Investigation, Methodology, Visualization, Writing – original draft, Writing – review & editing. **A.L. Nicusan:** Data curation, Formal analysis, Investigation, Software, Validation, Writing – original draft, Writing – review & editing. **C.R.K. Windows-Yule:** Conceptualization, Funding acquisition, Methodology, Project administration, Resources, Supervision, Writing – review & editing. **A. Ingram:** Conceptualization, Funding acquisition, Project administration, Resources, Supervision, Writing – review & editing. **D. Werner:** Data curation, Investigation, Methodology, Software, Validation. **S. Clifford:** Conceptualization, Funding acquisition, Project administration, Resources, Supervision, Writing – review & editing. **G.K. Reynolds:** Conceptualization, Funding acquisition, Project administration, Resources,Supervision, Writing – review & editing.

Declaration of competing interest

The authors declare the following financial interests/personal relationships which may be considered as potential competing interests: Owen Jones-Salkey reports financial support was provided by Engineering and Physical Sciences Research Council.

Data availability

Data will be made available on request.

Acknowledgements

References

Baxter, G., Olafsen, J., 2007. Experimental evidence for molecular chaos in granular gases. Phys. Rev. Lett. 99 (2), 028001.

Bekaert, B., Van Snick, B., Pandelaere, K., Dhondt, J., Di Pretoro, G., De Beer, T., Vervaet, C., Vanhoorne, V., 2022. In-depth analysis of the long-term processability of materials during continuous feeding. Int. J. Pharm. 614 (December 2021), 121454. http://dx.doi.org/10.1016/j.ijpharm.2022.121454.

Bhalode, P., Ierapetritou, M., 2020. A review of existing mixing indices in solid-based continuous blending operations. Powder Technol. 373, 195–209. http://dx.doi.org/10.1016/j.powtec.2020.06.043.

Boonkanokwong, V., Remy, B., Khinast, J.G., Glasser, B.J., 2016. The effect of the number of impeller blades on granular flow in a bladed mixer. Powder Technol. 302, 333–349. http://dx.doi.org/10.1016/j.powtec.2016.08.064, URL https://www.sciencedirect.com/science/article/pii/S0032591016305575?casa_token=ST4jsTngb-oAAAAA:aV8PqFfZ-1c3C-t5xLT_8xVrnBiy426HlqqXTNlNh01PmIT4IzHMjjt2Uy1YEeseQA271nptRjs#f0105.

Burcham, C.L., Florence, A.J., Johnson, M.D., 2018. Continuous manufacturing in pharmaceutical process development and manufacturing. Annu. Rev. Chem. Biomol. Eng. 9 (1), 253–281. http://dx.doi.org/10.1146/annurev-chembioeng-060817-084355.

Campbell, C.S., 1997. Self-diffusion in granular shear flows. J. Fluid Mech. 348, 85–101.

Che, H., Al-Shemmeri, M., Fryer, P.J., Lopez-Quiroga, E., Wheldon, T.K., Windows-Yule, K., 2023. PEPT validated CFD-DEM model of aspherical particle motion in a spouted bed. Chem. Eng. J. 453, 139689.

Ebrahimi, M., Yaraghi, A., Ein-Mozaffari, F., Lohi, A., 2018. The effect of impeller configurations on particle mixing in an agitated paddle mixer. Powder Technol. 332, 158–170. http://dx.doi.org/10.1016/j.powtec.2018.03.061, URL https://www.sciencedirect.com/science/article/pii/S0032591018302547?casa_token=Ilnk67Yn6nMAAAAA:ELDsV2aW51OEAxX3hzyUQoWl_Q2S7sg9OAHJ0CKLQ-Btl_Jsw9LBhtj0Ofe0sxNkBwdop3_Pc48#f0025.

Gao, Y., Ierapetritou, M., Muzzio, F., 2011a. Investigation on the effect of blade patterns on continuous solid mixing performance. Canadian J. Chem. Eng. 89 (5), 969–984. http://dx.doi.org/10.1002/cjce.20530, URL https://onlinelibrary.wiley.com/doi/10.1002/cjce.20530.

Gao, Y., Muzzio, F.J., Ierapetritou, M.G., 2012. Optimizing continuous powder mixing processes using periodic section modeling. Chem. Eng. Sci. 80, 70–80. http://dx.doi.org/10.1016/j.ces.2012.05.037, URL https://www.sciencedirect.com/science/article/pii/S0009250912003181?casa_token=ekRMR8ElnJ4AAAAA:8ju5z1WMyR3MIO9ry04pJwNXZfq3L-kUGr-Fa7ns3R-YNT9dWj6RiZYo6YCaRAoIIssTEKIr_PM.

Gao, Y., Vanarase, A., Muzzio, F., Ierapetritou, M., 2011b. Characterizing continuous powder mixing using residence time distribution. Chem. Eng. Sci. 66 (3), 417–425. http://dx.doi.org/10.1016/j.ces.2010.10.045.

Herald, M., Wheldon, T., Windows-Yule, C., 2021. Monte Carlo model validation of a detector system used for positron emission particle tracking. Nucl. Instrum. Methods Phys. Res. A 993, 165073.

International Council for Harmonisation of Technical Requirements for Pharmaceuticals for Human Use (ICH), 2012. Committee for Human Medicinal Products (CHMP) ICH Quality IWG Points to consider for ICH Q8/Q9/Q10 guidelines. Eur. Med. Agency 44 (February), URL www.ema.europa.eu.

International Council for Harmonisation of Technical Requirements for Pharmaceuticals for Human Use (ICH), 2023. ICH guideline Q13 on continuous manufacturing of drug substances and drug products. Eur. Med. Agency 31 (March), URL https://www.ema.europa.eu/en/ich-guideline-q13-continuous-manufacturing-drug-substances-drug-products-scientific-guideline.

Jones-salkey, O., Chu, Z., Ingram, A., Windows-yule, C.R.K., 2023. Reviewing the impact of powder cohesion on Continuous Direct Compression (CDC) Performance, cdc. pp. 1–48.

Lee, S.L., O'Connor, T.F., Yang, X., Cruz, C.N., Chatterjee, S., Madurawe, R.D., Moore, C.M., Yu, L.X., Woodcock, J., 2015. Modernizing pharmaceutical manufacturing: from batch to continuous production. J. Pharmaceutical Innov. 10 (3), 191–199. http://dx.doi.org/10.1007/s12247-015-9215-8.

Leimkuhler, B., Matthews, C., 2015. Molecular dynamics. Interdiscip. Appl. Math. 39, 443.

Martin, T., Seville, J., Parker, D., 2007. A general method for quantifying dispersion in multiscale systems using trajectory analysis. Chem. Eng. Sci. 62 (13), 3419–3428.

Megarry, A.J., Swainson, S.M., Roberts, R.J., Reynolds, G.K., 2019. A big data approach to pharmaceutical flow properties. Int. J. Pharm. 555 (October 2018), 337–345. http://dx.doi.org/10.1016/j.ijpharm.2018.11.059.

Morrison, A.J., Govender, I., Mainza, A.N., Parker, D.J., 2016. The shape and behaviour of a granular bed in a rotating drum using Eulerian flow fields obtained from PEPT. Chem. Eng. Sci. 152, 186–198. http://dx.doi.org/10.1016/j.ces.2016.06.022.

Mosig, J., Kleinebudde, P., 2015. Critical evaluation of root causes of the reduced compactability after roll compaction/dry granulation. J. Pharm. Sci. 104 (3), 1108–1118.

Nickerson, B., Kong, A., Gerst, P., Kao, S., 2018. Correlation of dissolution and disintegration results for an immediate-release tablet. J. Pharm. Biomed. Anal. 150, 333–340.

Nicuşan, A.L., Windows-Yule, C.R., 2020. Positron emission particle tracking using machine learning. Rev. Sci. Instrum. 91 (1), 13329. http://dx.doi.org/10.1063/1.5129251.

Palmer, J., Reynolds, G.K., Tahir, F., Yadav, I.K., Meehan, E., Holman, J., Bajwa, G., 2020. Mapping key process parameters to the performance of a continuous dry powder blender in a continuous direct compression system. Powder Technol. 362, 659–670. http://dx.doi.org/10.1016/j.powtec.2019.12.028.

Parker, D., Forster, R., Fowles, P., Takhar, P., 2002. Positron emission particle tracking using the new Birmingham positron camera. Nucl. Instrum. Methods Phys. Res. A 477 (1–3), 540–545.

Pernenkil, L., Cooney, C.L., 2006. A review on the continuous blending of powders. Chem. Eng. Sci. 61 (2), 720–742. http://dx.doi.org/10.1016/j.ces.2005.06.016.

Portillo, P.M., Vanarase, A.U., Ingram, A., Seville, J.K., Ierapetritou, M.G., Muzzio, F.J., 2010. Investigation of the effect of impeller rotation rate, powder flow rate, and cohesion on powder flow behavior in a continuous blender using PEPT. Chem. Eng. Sci. 65 (21), 5658–5668. http://dx.doi.org/10.1016/j.ces.2010.06.036.

Roth, W.J., Almaya, A., Kramer, T.T., Hofer, J.D., 2017. A demonstration of mixing robustness in a direct compression continuous manufacturing process. J. Pharm. Sci. 106 (5), 1339–1346. http://dx.doi.org/10.1016/j.xphs.2017.01.021.

Sarkar, A., Wassgren, C.R., 2009. Simulation of a continuous granular mixer: Effect of operating conditions on flow and mixing. Chem. Eng. Sci. 64 (11), 2672–2682. http://dx.doi.org/10.1016/j.ces.2009.02.011, URL https://www.sciencedirect.com/science/article/pii/S0009250909001080.

Siraj, M.S., 2014. Single-blade convective powder mixing: The effect of the blade shape and angle. Powder Technol. 267, 289–301. http://dx.doi.org/10.1016/j.powtec.2014.07.024, URL https://www.sciencedirect.com/science/article/pii/S0032591014006561#f0015.

Teżyk, M., Milanowski, B., Ernst, A., Lulek, J., 2015. Recent progress in continuous and semi-continuous processing of solid oral dosage forms: A review. Drug Dev. Ind. Pharmacy 42 (8), 1195–1214. http://dx.doi.org/10.3109/03639045.2015.1122607.

Tomita, Y., Nagato, T., Takeuchi, Y., Takeuchi, H., 2020. Control of residence time of pharmaceutical powder in a continuous mixer with impeller and scraper. Int. J. Pharm. 586, 119520. http://dx.doi.org/10.1016/j.ijpharm.2020.119520.

Van Snick, B., Holman, J., Vanhoorne, V., Kumar, A., De Beer, T., Remon, J.P., Vervaet, C., 2017. Development of a continuous direct compression platform for low-dose drug products. Int. J. Pharm. 529 (1–2), 329–346. http://dx.doi.org/10.1016/j.ijpharm.2017.07.003, http://www.sciencedirect.com/science/article/pii/S0378517317306026, https://linkinghub.elsevier.com/retrieve/pii/S0378517317306026.

Vanarase, A.U., Osorio, J.G., Muzzio, F.J., 2013. Effects of powder flow properties and shear environment on the performance of continuous mixing of pharmaceutical powders. Powder Technol. 246, 63–72. http://dx.doi.org/10.1016/j.powtec.2013.05.002.

Vanhoorne, V., Vervaet, C., 2020. Recent progress in continuous manufacturing of oral solid dosage forms. Int. J. Pharm. 579, http://dx.doi.org/10.1016/j.ijpharm.2020.119194.

Wahlich, J., 2021. Review: Continuous manufacturing of small molecule solid oral dosage forms. Pharmaceutics 13 (8), http://dx.doi.org/10.3390/pharmaceutics13081311.

Werner, D., Davison, H., Robinson, E., Sykes, J., Seville, J., Wellings, A., Bhattacharya, S., Monsalve, D.S., Wheldon, T.K., Windows-Yule, C., 2023. Effect of system composition on mixing in binary fluidised beds. Chem. Eng. Sci. 118562.

Wildman, R., Hansen, J.-P., Parker, D., 2002. Velocity auto-correlation functions in three-dimensional vibro-fluidized granular beds. Phys. Fluids 14 (1), 232–239.

Wildman, R., Huntley, J., Hansen, J.-P., Parker, D., Allen, D., 2000. Single-particle motion in three-dimensional vibrofluidized granular beds. Phys. Rev. E 62 (3), 3826.

Windows-Yule, C., Herald, M., Nicuşan, A., Wiggins, C., Pratx, G., Manger, S., Odo, A., Leadbeater, T., Pellico, J., de Rosales, R.T., et al., 2022a. Recent advances in positron emission particle tracking: A comparative review. Rep. Progr. Phys. 85 (1), 016101.

Windows-Yule, C., Neveu, A., 2022. Calibration of DEM simulations for dynamic particulate systems. Pap. Phys. 14, 140010.

Windows-Yule, K., Nicuşan, L., Herald, M.T., Manger, S., Parker, D., 2022b. Positron Emission Particle Tracking. IOP Publishing.

Windows-Yule, C., Rosato, A., Rivas, N., Parker, D., 2014. Influence of initial conditions on granular dynamics near the jamming transition. New J. Phys. 16 (6), 063016.

Windows-Yule, C., Seville, J., Ingram, A., Parker, D., 2020. Positron emission particle tracking of granular flows. Annu. Rev. Chem. Biomol. Eng. 11, 367–396.

Windows-Yule, C., Tunuguntla, D.R., Parker, D., 2016. Numerical modelling of granular flows: A reality check. Comput Part. Mech. 3, 311–332.

Yang, Z., Fryer, P., Bakalis, S., Fan, X., Parker, D., Seville, J., 2007. An improved algorithm for tracking multiple, freely moving particles in a positron emission particle tracking system. Nucl. Instrum. Methods Phys. Res. A 577 (3), 585–594.

Zheng, C., Li, L., Nitert, B.J., Govender, N., Chamberlain, T., Zhang, L., Wu, C.Y., 2022. Investigation of granular dynamics in a continuous blender using the GPU-enhanced discrete element method. Powder Technol. 412 (July), 117968. http://dx.doi.org/10.1016/j.powtec.2022.117968.